Journal of Biomolecular NMR, **14:** 345–356, 1999.
KLUWER/ESCOM

^{1}H-^{15}N NMR dynamic study of an isolated α-helical peptide (1–36)-bacteriorhodopsin reveals the equilibrium helix-coil transitions

Vladislav Yu. Orekhov[a,b], Dmitry M. Korzhnev[a], Tammo Diercks[c], Horst Kessler[c] & Alexander S. Arseniev[a,*]

[a]*Shemyakin and Ovchinnikov Institute of Bioorganic Chemistry, Russian Academy of Sciences, Ul. Miklukho-Maklaya 16/10, 117871 Moscow, Russia;* [b]*Biochemistry and Biophysics, Lundberg Laboratory, Göteborg University, Box 462, SE 405 30 Göteborg, Sweden;* [c]*Institut für Organische Chemie und Biochemie, Technische Universität München, Lichtenbergstrasse 4, D-85747 Garching, Germany*

Received 13 April 1999; Accepted 24 June 1999

Key words: alpha helix, anisotropy, bacteriorhodopsin, CSA, hydrogen bond, random coil, relaxation

Abstract

The backbone dynamics of the bacteriorhodopsin fragment (1–36)BR solubilized in a 1:1 chloroform/methanol mixture were investigated by heteronuclear ^{1}H-^{15}N NMR spectroscopy. The heteronuclear ^{15}N longitudinal and transverse relaxation rates and ^{15}N{^{1}H} steady-state NOEs were measured at three magnetic fields (11.7, 14.1, and 17.6 T). Careful statistical analysis resulted in the selection of the extended model-free form of the spectral density function [Clore et al. (1990) *J. Am. Chem. Soc.*, **112**, 4989–4991] for all the backbone amides of (1–36)BR. The peptide exhibits motions on the micro-, nano-, and picosecond time scales. The dynamics of the α-helical part of the peptide (residues 9–31) are characterised by nanosecond and picosecond motions with mean order parameters $S_s^2 = 0.60$ and $S_f^2 = 0.84$, respectively. The nanosecond motions were attributed to the peptide's helix-coil transitions in equilibrium. Residues 3–7 and 30–35 also exhibit motions on the pico- and nanosecond time scales, but with lower order parameters. Residue 10 at the beginning of the α-helix and residues 30–35 at the C-terminus are involved in conformational exchange processes on the microsecond time scale. The implications of the obtained results for the studies of helix-coil transitions and the dynamics of membrane proteins are discussed.

Introduction

The most widely accepted theory of protein folding contends that it is a hierarchical process. Models such as the diffusion-collision model (for a review see Karplus and Weaver, 1994) and the framework model (reviewed by Baldwin, 1989) suggest that secondary structure elements serve as building blocks for the construction of the native tertiary structure. In both models, elements of secondary structure are formed during the early stages of the folding process and subsequently assembled into the three-dimensional protein structure. For membrane proteins this two-stage view of protein folding is supported by numerous experimental studies on the reconstruction of functional bacteriorhodopsin from its independently folded α-helical fragments in lipid bilayers (Popot et al., 1987; Kahn and Engelman, 1992; Marti, 1998). Various NMR studies (reviewed by Pervushin and Arseniev, 1995a) have shown that individual α-helical fragments of bacteriorhodopsin can acquire and retain their native-like structure in membrane-mimicking media without long-range tertiary interactions with other parts of the protein. The individual α-helices in the membrane-mimicking environment might also be a useful model for understanding dynamics and folding mechanisms of membrane proteins.

While there has been progress in understanding the thermodynamics of the helix-coil transition in aqueous solutions (Chou and Scheraga, 1971; Scholtz and

*To whom correspondence should be addressed. E-mail: aars@nmr.ru.

Baldwin, 1992), its kinetics have been studied less extensively. Since the mid-1960s, different experimental techniques were used to elucidate the kinetics of helix-coil transitions (reviewed by Gruenewald et al., 1979). For homopolymers of high molecular weight in aqueous solutions, these studies yielded averaged midpoint transition times between ca. 50 ns and several microseconds. Recently, a new laser-induced temperature-jump technique (Phillips et al., 1995) was applied to study the helix-coil transition kinetics on short alanine-based peptides in water (Williams et al., 1996; Thompson et al., 1997). It provided unique experimental insights into fast transitions on a time scale of tens to hundreds of nanoseconds. However, the time range from picoseconds to several nanoseconds, which is thought to correspond to the primary events of helix-coil transitions (e.g. see Daggett and Levitt, 1992; Korzhnev et al., 1999a and references cited therein), is still beyond experimental access.

Usually, helical peptides in water exhibit low cooperativity for thermal unfolding processes (Scholtz and Baldwin, 1992). Consequently, one should expect relatively high populations of partially unfolded states even much below the critical temperature for thermal unfolding. A study of the equilibrium dynamics of interconversion of different helical species could provide valuable insights into the kinetics of the helix-coil transition. The nanosecond dynamics of the helix-coil interconversion equilibrium were recently elucidated by electron spin resonance spectroscopy (ESR) on a series of alanine-based peptides in aqueous solution (Miick et al., 1993). It was shown that even in a 1:4 TFE/water mixture, where circular dichroism data indicate very high populations for the α-helix, the peptides exhibit significant local helix-coil transitions at the helix termini.

Low polar solvents like trifluoroethanol, methanol, or mixtures of chloroform and methanol are commonly used to mimick a membrane environment. In comparison to water, these membrane-mimicking solvents are known to increase the helix content in peptides (for a review see Hirota et al., 1997) while markedly reducing the cooperativity of the helix-coil transitions (Luo and Baldwin, 1997), which produces a wide range of partially unfolded α-helical states in equilibrium. The solution of the system of kinetic equations for the α-helical peptide (9–31)BR in nonpolar solvents (Korzhnev et al., 1999b) has produced a spectrum of helix-coil transition times, ranging from 10^{-10} to 10^{-6} s, which can be divided into two parts. The faster transitions occur with a nearly continuous distribution of transition times (10^{-10}–10^{-8} s) and are associated with the interconversion between various helical states, such as the elongation or shortening of an α-helix by one or several residues. The slower transitions, on the other hand, occur with few discrete transition times (10^{-7}–10^{-6} s). They correspond to interconversions between the denatured (all-coil) state and some partially folded (helical) conformations and involve several residues simultaneously whereas the fast transitions usually affect only individual residues. Both classes of transitions fall within time ranges that are amenable to detection via NMR relaxation measurements.

Modern heteronuclear NMR spectroscopy is a powerful tool for studying protein dynamics in a wide time range (for a review see Palmer et al., 1996). Detailed site-specific information on amplitudes and correlation times of internal motions can be obtained from the measurement of backbone amide ^{15}N relaxation rates, provided these internal motions are of the order of or faster than the overall molecular tumbling. Since the effective rotation correlation time for short α-helical peptides in solution is in the nanosecond time range, NMR studies of such peptides could provide the experimental data on helix-coil transition kinetics in the critical time range from picoseconds to several nanoseconds where real-time experiments fail because of dead time limitations.

In this work, we study the internal dynamics of the bacteriorhodopsin fragment (1–36) which forms a stable α-helix over residues 9–32 (Pervushin and Arseniev, 1992). Since we were particularly interested in the dynamics on the nanosecond time scale (Korzhnev et al., 1997) close to the correlation time for the overall molecular tumbling, measurements at three magnetic fields were performed to ascertain the required statistical confidence and resolution for the sampling of the spectral density function.

Materials and methods

Sample preparation and NMR measurements

Uniformly ^{15}N-labelled (1–36)BR was obtained as described previously (Orekhov et al., 1995). Dry peptide (3 mg) was dissolved in 0.5 ml of a 1:1 (volume ratios) mixture of deuterated chloroform and methanol-d_3 and 0.1 M $^{2}HCO_2NH_4$ buffer. The final concentration of the peptide in the sample was ca. 1.5 mM. The apparent pH in methanol was 4.9. NMR experiments were performed on four spectrometers: Varian Unity-

plus and Unity (^{1}H Larmor frequencies of 500 and 600 MHz, respectively) and Bruker DMX spectrometers (^{1}H Larmor frequencies of 600 and 750 MHz, respectively).

A series of ^{1}H-detected two-dimensional correlation spectra for the measurement of the backbone ^{15}N longitudinal and transverse relaxation rates, R_1 and R_2, and the heteronuclear ^{15}N{^{1}H} steady-state NOE were acquired using the pulse sequences described by Farrow et al. (1994). The parameters used in the different experiments are summarised in Table 1. T_2 experiments were recorded with a CPMG echo delay of 1 ms between ^{15}N inversion pulses of 70–90 μs. The total acquisition time per relaxation measurement was 15–20 h. No presaturation of the intense OH signal from methanol was performed in either experiment. In the experiments for measuring longitudinal and transverse relaxation rates the OH magnetisation was dephased by pulsed field gradients. In the NOE experiment the OH magnetisation was flipped back to +z prior to the acquisition with the residual OH magnetisation in the transverse plane being dephased by the field gradients.

Importance of the temperature control

In all NMR experiments special attention was paid to the actual temperature of the sample. Even small changes in the temperature during one experiment or between different experiments can lead to substantial bias in relaxation data, due mostly to the temperature dependence of the solvent viscosity (ca. 3% per K). Neglecting temperature-dependent changes in the internal dynamics, the changes in viscosity lead to altered rotational diffusion rates resulting in relative biases of comparable order (ca. 3% per K) in the measured longitudinal and transverse relaxation rates.

For all spectrometers the temperature of 303 K was adjusted using the temperature-dependent ^{1}H chemical shift difference of pure methanol (VanGeet, 1970). For the (1–36)BR sample in the chloroform-methanol mixture, the position of the methanol OH signal was used as a sensitive internal indicator for monitoring the sample temperature during the experiments. Note that the deuterium signal of the methanol methyl group was used to lock the magnetic field of the spectrometer. The position of the OH signal was obtained from a one-dimensional proton spectrum recorded in one scan immediately after the termination of a 30–40 min test run of the respective relaxation experiment. The delay between the termination of the test run and the measurement of the OH signal position was less than two seconds, assuring that the actual temperature during the relaxation experiment was recorded.

Radio frequency irradiation during an NMR experiment can cause substantial heating of the sample, resulting in different effective sample temperatures for different experiments, with the consequences for relaxation data precision discussed above. This effect may introduce a significant bias in the extracted relaxation parameters. Several approaches can be considered to avoid possible temperature artefacts: (i) all spectra of different mixing times can be recorded separately with individual temperature corrections; this approach, however, can result in artefacts due to spectrometer and sample instabilities during long experiments; (ii) additional delays and/or off-resonance irradiation can be introduced into the pulse sequences in order to equalise the heat dissipation for different mixing times (Bracken et al., 1999); (iii) in our measurements, we relied on the averaging of temperature fluctuations as explained below.

The mean sample temperature during an NMR experiment results from the balance between radio frequency heating and energy absorption by the cooling air. The time constant for the equilibration of this process is governed by the geometry of the probehead and the sample as well as by the flow rate of the cooling gas, but does not depend on the irradiation power. This time constant can be roughly estimated from the change in the lock signal amplitude at the beginning of NMR experiments using significant irradiation. From our experience it follows that this time constant is not less than tens of seconds. Thus, the temporary changes in sample irradiation for different mixing times are efficiently averaged out and do not lead to significant temperature fluctuations provided they occur fast enough and periodically. In our experiments, these requirements were met by interleaved acquisition where mixing times were alternated after each scan such that long and short mixing times were grouped pairwise. Since the duration of a single scan is ca. 2–4 s, the frequency of alternation was sufficiently fast for good averaging of the temperature. It is notable that radio frequency irradiation sometimes results in the apparent cooling of the sample. This can happen if the temperature control sensor, which is commonly located very close to the frequency coils in the probehead, is more sensitive to the irradiation than the sample itself. This effect, however, can also be compensated for by an appropriate setting of the temperature unit. In the case of (1–36)BR, the sample heating monitored as described above was ca. 0.3,

Table 1. Experimental parameters used in the experiments for determining backbone ^{15}N longitudinal and transverse relaxation rates, R_1 and R_2, respectively, and heteronuclear $^{15}N\{^1H\}$ NOEs. Experiment type, spectrometer type, recovery delay (D1), number of complex points acquired in the indirect dimension (TD1), set of relaxation delays, and number of measurements (m) are presented for each experiment

Exp. type	Spectrometer	D1 (s)	TD1[a]	Relaxation delays (ms)	m
R_1	Unity+ 500	1.6	60	15,80,120,200,300,400,500,700,900,1000	1
R_1	Unity 600	2.0	54	10,50,100,200,300,400,600,800,1000	2
R_1	DRX 600	2.0	64	16,33,49,66,98,131,196,262,394,525,787	2
R_1	DRX 750	1.4	96	16,31,62,124,186,248,372,497,745,933,1490	2
R_2	Unity+ 500	1.6	60	5,41,77,113,149,185,220,256,292,328,364,400	1
R_2	Unity 600	2.0	60	0,16,32,48,80,112,144,176,1922	
R_2	DRX 600	2.0	64	16,32,48,64,80,95,112,128,144,159,176,192	2
R_2	DRX 750	2.0	55	16,32,47,64,80,95,111,127,143,159,175,206	1
NOE	Unity+ 500	3.5[b]	56		1
NOE	Unity 600	4.5[b]	80		2
NOE	DRX 600	4.5[b]	64		2
NOE	DRX 750	4.5[b]	80		2

[a]The spectral widths in the ω_1 direction were 1200, 1400, 2000 Hz for the spectrometers with ^1H Larmor frequencies of 500, 600 and 750 MHz, respectively.
[b]In all $^{15}N\{^1H\}$-NOE experiments two spectra were acquired with and without proton presaturation, respectively. In the former case, the relaxation delay was substituted by a proton presaturation time of the same length.

0.1, and less than 0.1 K for the T_2, NOE, and T_1 experiments, respectively. Since the precision of the calibration and the stability of the temperature units were about 0.1 K, an appropriate temperature compensation was performed only for the T_2 and in some cases for the NOE measurements. In conclusion, the sample temperature during one experiment was stable to within 0.1 K and differred for not more than 0.2 K between different experiments, resulting in an uncertainty of 0.5% for the relaxation rates on the assumption that only the temperature dependence of the solvent viscosity needs to be taken into account.

Evaluation of the spectra

All spectra were processed and quantified using a macro within the VNMR software. Bruker spectra were first converted to VNMR format. In each dimension, time domain data was zero-filled twice and a non-shifted Gaussian weighting function was applied for apodization prior to the Fourier transform. Suppression of the strong OH signal of methanol was excellent and experiments were adjusted such that the spectra required no first order phase correction in either dimension, assuring that no baseline correction was necessary. Peak intensities were measured using supplementary home-written software. Both extraction of relaxation times from exponential curve fit to a two-parameter function (an offset compensation proved unnecessary) and model-free analysis of relaxation data were performed with the home-written software DASHA (Orekhov et al., 1996). Relaxation rates and NOEs from several experiments (see Table 1) were averaged. For each averaged relaxation rate (T_1, T_2, NOE) the uncertainties were taken to be the maximum of the following three values: (i) the dispersion in a set of redundant measurements; (ii) the uncertainties obtained from the covariance matrix of the least-squares fit of the exponential decay curves and from a Monte Carlo process (T_1- and T_2-experiments), or from the signal-to-noise ratios ($^{15}N\{^1H\}$-NOE experiments), respectively; and (iii) minimal uncertainties of 2% for T_1 and T_2 and ± 0.05 for the NOE, accounting for possible small (systematic) errors in the experimental data and in the physical constants and expressions governing the relaxation processes.

Model-free analysis

Dynamic models

A typical set of heteronuclear NMR relaxation data consists of the longitudinal R_1 and transverse R_2 relaxation rates and the heteronuclear NOE sampled at one or several magnetic fields. Their corresponding theoretical values can be back-calculated using standard expressions (Abragam, 1961) and different forms of the autocorrelation function, C(t). This function com-

prises all information on the NH vector dynamics of the backbone amide group occurring on the pico- to nanosecond time scale.

If the molecular rotation is isotropic and uncorrelated with the internal motions, the total correlation function C(t) can be rigorously factorized into a product of internal $C_I(t)$ and overall $C_O(t)$ correlation functions (Lipari and Szabo, 1982):

$$C(t) = C_I(t)C_O(t) \quad (1)$$

Although this factorization is not valid in the case of anisotropic overall rotation, it was shown to be a good approximation (Lipari and Szabo, 1982) and is implied in the following. A short description of the models of internal and overall motions considered in this article can be found in Table 2. All model-free calculations were performed with a ^{1}H–^{15}N internuclear distance (R_{HN}) of 0.102 nm and a ^{15}N chemical shift anisotropy (^{15}N-CSA) of -170 ppm. These two parameters were subsequently allowed to vary during minimizations (see below) in order to verify whether their adjustment within reasonable limits could significantly improve the agreement between experimental and calculated relaxation data. R_2 values may additionally be increased by conformational exchange processes on the micro- to millisecond time scale. These relaxation contributions are proportional to the square of the magnetic field (Reeves, 1975) and can be accounted for by a single parameter Δ_{ex}, corresponding to the additional line broadening (in Hz) at 17.6 T magnetic field strength.

Model evaluation and statistical analysis

In order to extract spatial and temporal characteristics of internal motions, the experimental relaxation rates and NOEs are fitted to the theoretical values by minimizing the per residue loss function χ^2 (e.g., Mandel et al., 1995; Orekhov et al., 1995):

$$\chi^2(\zeta) = \sum_{i=1}^{N} \frac{\left(V_i^{th}(\zeta) - V_i^{\exp}\right)^2}{\left(\Delta V_i^{\exp}\right)^2} \quad (2)$$

$V^{th}(\zeta)$ and $V^{\exp}$ are the theoretical and experimental relaxation values, respectively; $\Delta V^{\exp}$ is the corresponding uncertainty in the experimental value; index i runs over the set of N experimentally determined relaxation rates and NOEs for the given residue (for T_1, T_2, and NOEs measured at three magnetic fields we have $N = 9$), and ζ denotes the set of k adjustable model parameters (which can include the conformational exchange term Δ_{ex} for some residues). The *cumulative* loss function is the sum of several per residue loss functions. It is generally used for the optimization of global parameters (e.g. parameters of the global molecular rotational tumbling) and for the detection of general systematic discrepancies between experimental data and a model.

If experimental errors are small, normally distributed, and uncorrelated with each other, the minimum for $\chi^2(\zeta)$ should correspond to the chi-square distribution with (N−k) degrees of freedom. The appropriateness of a particular model can then be evaluated by calculating the chi-square probability for obtaining a loss function higher or equal to the one calculated from Equation 2. Strictly speaking, the chi-square statistics is not applicable to non-linear regression analysis. However, our Monte Carlo simulations showed that chi-square statistics provides almost exact probabilities provided the model parameters do not approach their limiting values (e.g. 1 for the order parameter). Commonly, a model is taken to be inappropriate if the loss function exceeds some critical value defined by a given probability (usually the 95% quantile) for randomly obtaining a higher loss function. For large numbers of degrees of freedom (i.e. greater than ca. 20–30) this critical value approaches the number of degrees of freedom. If several models with different numbers of adjustable parameters have to be compared, the application of the pairwise F-test is very helpful (Mandel, 1995). This test addresses the question of whether the reduction in the loss function obtained for a model with more parameters is statistically significant. The F-test is less sensitive to the chosen uncertainties $\Delta V^{\exp}$ since it essentially compares the ratio of the loss functions for two models.

The dynamic model for the internal motions of a particular backbone amide $^{15}N-^1H$ vector was selected according to the following procedure. Minimizations of the per residue loss function were performed for each of the four models of internal motions (models I–IV in Table 2) with and without consideration of a conformational exchange contribution, Δ_{ex}, resulting in a total of 8 minimizations per residue. The parameters of the overall rotational diffusion were kept constant (see below). Then, those models yielding a loss function higher than the critical 95% quantile were rejected while the simplest model (with the lowest number of adjustable parameters), which provided a loss function below the critical level, was accepted. In all cases, an additional F-test for the 90% quantile confirmed our choice of the model function.

Table 2. Autocorrelation functions and their adjustable parameters[a]

Type	Abbreviation used in the text	Adjustable parameters [b]	Reference	Motional model and time scale
$C_I(t)$	I	S^2	Lipari and Szabo, 1982	Very fast internal dynamics
$C_I(t)$	II	S^2, τ_e	Lipari and Szabo, 1982	Picosecond internal dynamics
$C_I(t)$	III	S_f^2, S_s^2, τ_s	Clore et al., 1990	Intermediate internal dynamics in nanoseconds
$C_I(t)$	IV	S_f^2, S_s^2, τ_s, τ_f	Clore et al., 1990	Intermediate internal dynamics in pico- and nanoseconds
$C_O(t)$	Isotropic (Is)	τ_R	Lipari and Szabo, 1982	Isotropic overall tumbling
$C_O(t)$	Axial symmetry (AxS)	τ_R, $D_\perp/D_{\|\|}$, α, β	Woessner, 1962	Anisotropic tumbling of a cylindrical molecule
$C_O(t)$	Full anisotropy (FlA)	τ_R, D_1/D_3, D_2/D_3, α, β, γ	Woessner, 1962	Anisotropic tumbling of a molecule of arbitrary shape

[a] S^2, S_f^2, and S_s^2 are the order parameters for overall, fast (correlation time less than ca. 10 ps), and intermediate (correlation time in the nanosecond time range) internal motions, respectively; τ_e (or τ_f) and τ_s are the correlation times for fast and intermediate local motions, respectively; $D_i (i = 1, 2, 3)$ are the eigenvalues of the rotation diffusion tensor; $D_\perp = D_1 = D_2$ and $D_{||} = D_3$; α, β, and γ are Euler angles for the transformation of molecular coordinates into the eigenbase of the molecular rotation diffusion tensor. The effective correlation time for the anisotropic overall tumbling, comparative to the isotropic model, is defined as $\tau_R = [2(D_1 + D_2 + D_3)]^{-1} = [(4D_\perp + 2D_{||})]^{-1}$.

[b] An explicit form for the different types of the autocorrelation functions can be found elsewhere (see the literature cited).

Evaluation of the overall rotation correlation time

The overall rotation correlation time (τ_R) was obtained as a global adjustable parameter from minimization of the *cumulative* loss function for residues 9–31 which form the α-helix in (1–36)BR. For the calculation of τ_R it was assumed that the dynamics of all amides in the α-helix 9–31 can be described by a common model function. This approximation is justified by the common structural element and the very similar relaxation data of these residues. The calculations were repeated for different model functions and the cumulative loss functions obtained from these minimizations were compared statistically using chi-square and F-tests. The final τ_R value was taken from the most appropriate model (see Results).

If model I (see Table 2) is valid for the majority of backbone amide HN vectors, the value of τ_R can be readily calculated from the ^{15}N R_1/R_2 ratio (Kay et al., 1989) since this ratio is independent from the only parameters of the internal motions, S^2. In the presence of significant nanosecond motions involving most of the residues, however, τ_R as calculated from the R_1/R_2 ratio is underestimated (Korzhnev et al., 1997). The subsequent model-free analysis will then be biased towards the premise of the implied 'fast' model function, i.e. producing the erroneous impression of fast internal motions. With the correct value of τ_R, however, the discrimination between the fast models I and II and model III allowing nanosecond motions is straightforward from a comparison of the loss functions χ^2. Usually, model III requires a significantly longer (10–20%) overall correlation time, but in practice neither model I, II nor III can be rejected on the basis of statistical chi-square or *F*-tests for relaxation data acquired at just one magnetic field if the overall rotation correlation time is unknown.

If experimental relaxation data are available for several magnetic fields, χ^2values become more sensitive to the differences between models I, II and III. Computer simulations have shown that a decrease in the apparent τ_R derived from the R_1/R_2 ratio at higher magnetic fields can serve as a clear indicator for model III (Korzhnev et al., 1997).

Hydrodynamic calculations

Hydrodynamic calculations for the α-helical fragment (residues 9–31) were performed using the DIFFC module implemented in the DASHA software package. The beads approach (Garcia de la Torre and Bloomfield, 1981) was applied with the backbone C^α atoms at the centre of the beads of radius 0.35 nm. These calculations yielded the principal axes and eigenvalues of the rotation diffusion tensor. Note that a precise setting of the microscopic solvent viscosity (which scales the rotational correlation time) was not important since the effective overall rotation correlation time was later adjusted through minimization of the cumulative loss function.

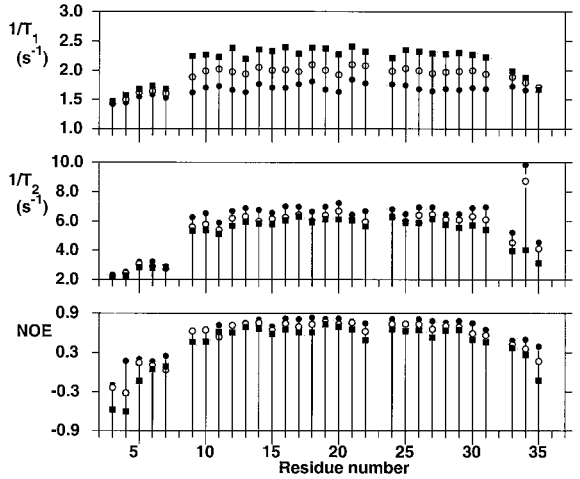

Figure 1. Experimental longitudinal and transverse ^{15}N relaxation rates and heteronuclear ^{15}N{^{1}H} steady-state NOE of (1–36)BR. The relaxation data was measured at three magnetic fields with ^{1}H Larmor frequencies of 500, 600, and 750 MHz (filled circles, open circles, and filled squares, respectively). Uncertainties of the experimental values are shown as grey bars.

Results

Relaxation data

Of the 35 backbone amide groups, 31 were evaluated in the relaxation measurements. (1–36)BR contains one proline (Pro8). Two pairs of signals were overlapped (Gly16 and Gly23, and Lys30 and Met32). As all of these residues fall within the same structural motif (α-helix), similar dynamical behaviour can be expected. We therefore evaluated these overlapped peaks as well and arbitrarily assigned the apparent relaxation rates to Gly16 and Lys30, respectively. Signal-to-noise ratios were different for the individual signals and in different experiments, but were never less than ca. 20–30 with typical values of ca. 50. This resulted in very small, usually less than 1%, uncertainties of the T_1 and T_2 values obtained in the exponential fit procedure using the covariance matrix. For most of the amide nitrogens the final uncertainties of R_1, R_2 and the ^{15}N{^{1}H}NOEs were set to the assumed minimal uncertainties (see Materials and methods for details). The results for the measurements of ^{15}N R_1, R_2, and the ^{15}N{^{1}H}-NOE are shown in Figure 1.

Overall correlation time and selection of the model-free spectral density function

Significant parts of the N- and C-terminal regions of (1–36)BR are known to be disordered under the conditions of our experiments (Pervushin et al., 1992). We therefore restricted the initial estimation of the overall rotation correlation time to the α-helical part (residues 9–31). Results of the fit of different forms of the spectral density function to the experimental data are summarised in Table 3. In each calculation, the overall rotation correlation time was adjusted as a free global parameter. As can be seen from the values of the loss function listed in Table 3, models I and II (lines 1 and 8 in Table 3, respectively) cannot fit the experimental data well. Only model III (line 15 in Table 3), accounting for local nanosecond motions, affords reasonable correspondence with the experiment.

Although the statistical tests unambiguously favour model III, further aspects in the evaluation of the best model function must be taken into consideration: (i) the anisotropy of the overall molecular tumbling; (ii) conformational exchange processes on the micro- to millisecond time scale; and (iii) uncertainties in the physical constants used in the relaxation analysis (notably the ^{15}N-CSA and ^{1}H–^{15}N distance).

It was shown that the neglect of anisotropy for the overall molecular rotation can misleadingly suggest local nanosecond motions (Schurr et al., 1994). The hydrodynamic calculations for the single helical (8–32)BR fragment yield an axially symmetric rotational diffusion tensor with eigenvalue ratios of 1:0.296:0.297 and the long axis lying almost parallel to the axis of the α-helix. The HN vectors of the backbone amides in the α-helix also nearly coincide with the helix axis, forming an angle of only $21 \pm 11°$ with the longest axis of the diffusion tensor. An examination of Woessner's (1962) expressions shows that the molecular rotation correlation function in this case is essentially mono-exponential with the effective correlation times for the individual HN vectors not differing much. Actually, the ^{15}N relaxation rates and NOEs for the backbone amides in an isolated ideal α-helix can to a good approximation be reproduced by the isotropic form of the overall rotation correlation function (Orekhov et al., 1995). It was also recently shown (Beloborodov et al., 1998) that the coupling between translation and rotation diffusion does not affect NMR relaxation rates even in the case of screw-shaped molecules like an α-helix. It is therefore not surprising that the consideration of rotation diffusion anisotropy for (1–36)BR does not significantly improve the quality of the fit for either model (lines 7, 14, and 20 in Table 3). The only and obvious difference with respect to the isotropic case is the reduction of the effective rotation correlation time, which for anisotropic mod-

Table 3. Results of model-free calculations for determining τ_R. Only residues 9–31 of the α-helix of (1–36)BR were used for these calculations

Run #	Model[a]	Adjustable parameters (mean values)	Optimised τ_R (ns)	Principal axes ratio	Degrees of freedom	Cumulative χ^2
1	Is, I,	τ_R, S^2 (0.81),	4.40 ± 0.03		175	995
2	Is, I	τ_R, S^2(0.76), CSA(191 ppm)	4.40 ± 0.03		153	888
3	Is, I	τ_R, S^2(0.92), R_{HN}(0.105 nm)	4.40 ± 0.03		154	897
4	Is, I	τ_R, S^2(0.77), Δ_{ex}(1.08 Hz)[b]	3.96 ± 0.06		153	642
5	FlA, I	τ_R, S^2(0.82)	2.74 ± 0.03	0.296, 0.297[c]	175	2417
6	AxS, I	τ_R, S^2(0.81)	4.08 ± 0.05	0.182 ± 0.008,	172	485
7	FlA, I	τ_R, D_1/D_2, D_2/D_3, α, β, γ, S^2(0.81)	4.18 ± 0.07	0.14 ± 0.02, 0.20 ± 0.01	170	471
8	Is, II	τ_R, S^2(0.79), τ_e(0.041 ns)	4.48 ± 0.02		154	574
9	Is, II	τ_R, S^2(0.72), τ_e(0.034 ns), CSA(200 ppm)	4.50 ± 0.03		131	380
10	Is, II	τ_R, S^2(0.78), τ_e(1.7 ns), R_{HN}(0.106 nm)	5.02 ± 0.07		131	141
11	Is, II	τ_R, S^2(0.77), τ_e(0.032 ns), Δ_{ex}(0.82 Hz)[b]	4.13 ± 0.05		132	320
12	FlA, II	τ_R, S^2(0.81), τ_e(0.040 ns)	2.79 ± 0.03	0.296, 0.297[c]	157	1950
13	AxS, II	τ_R, $D_\perp/D_{\|\|}$, α, β, S^2(0.79), τ_e (0.021 ns)	4.38 ± 0.05	0.22 ± 0.01	155	317
14	FlA, II	τ_R, D_1/D_2, D_2/D_3, α, β, γ, S^2(0.79), τ_e(0.021 ns)	4.54 ± 0.07	0.16 ± 0.02, 0.24 ± 0.01	153	292
15	Is, III	τ_R, S_f^2(0.84), S_s^2(0.61), τ_s(2.9 ns)	5.77 ± 0.15		131	120
16	Is, III	τ_R, S_f^2(0.83), S_s^2(0.70), τ_s(2.4 ns), CSA(176 ppm)	5.33 ± 0.15		109	95
17	Is, III	τ_R, S_f^2(0.88), S_s^2(0.65), τ_s(2.7 ns), R_{HN}(0.103 nm)	5.54 ± 0.15		111	98
18	Is, III	τ_R, S_f^2(0.81), S_s^2(0.42), τ_s(4.2 ns), τ_f(0.016 ns),	6.9 ± 0.2		116	103
19	Is, III	τ_R, S_f^2(0.84), S_s^2(0.64), τ_s(2.8 ns), Δ_{ex}(0.24 Hz)[b]	5.45 ± 0.15		116	98
20	FlA, III	τ_R, S_f^2(0.84), $S_s^2$0.66), τ_s(2.6 ns)	3.52 ± 0.05	0.296, 0.297[c]	131	154
21	AxS, III	τ_R, $D_\perp/D_{\|\|}$, α, β,S_f^2(0.83), S_s^2(0.76), τ_s(3.0 ns)	5.2 ± 0.4	0.28 ± 0.01	129	117
22	FlA, III	τ_R, D_1/D_2, D_2/D_3, α, β, γ, S_f^2(0.83), S_s^2(0.8), τ_s(2.9 ns)	5.1 ± 0.4	0.22 ± 0.04, 0.31 ± 0.03	128	116

[a] See Table 2 for the definition of the models.
[b] Δ_{ex} values (in Hz) refer to a magnetic field strength of 17.6 T.
[c] Anisotropy parameters obtained from the hydrodynamic calculations were kept constant in these minimisations.

els corresponds to the average of all correlation time eigenvalues.

It is notable that if the parameters defining the anisotropy of the molecular rotation are allowed to vary during the minimisation, the loss function can drop considerably (see lines 6, 7, 13, and 14 in Table 3) for models I and II. This merely reflects the operational similarity between the anisotropic calculations and the application of model III (Schurr et al., 1994). Both motional models presume at least two correlation times on the nanosecond time scale which are, however, attributed to different sources: in the anisotropic model these correlation times are attributed to the global tumbling alone, while the isotropic model attributes them to global and internal motions, respectively. Since all HN vectors of α-helical amides are aligned almost parallel, resulting in one common effective correlation time, and since the relaxation data does not exhibit large variations, both approaches produce indistinguishable spectral density functions J(ω). The anisotropic model, however, is not consistent with the anticipated hydrodynamic behaviour of the (8–32)BR α-helix as the optimised orientation of the symmetry axis of the diffusion tensor (lines 6 and 13 in Table 3) after minimisation lies nearly perpendicular to the helix axis, with the HN vectors forming angles of $87 \pm 12°$ with the symmetry axis.

Conformational exchange on the micro- to millisecond time scale can substantially increase the apparent transverse relaxation rates. Results of the calculations with consideration of conformational exchange are presented in lines 4, 11, and 19 of Table 3. Clearly, these calculations afford a significant reduction of the loss function especially for models I and II. However, model III still provides a statistically meaningful improvement over models I and II. Moreover, if model III is chosen, the exchange term is required only for a few residues. Thus, conformational exchange cannot account for the poor fit of models I and II.

The analysis of NMR relaxation data furthermore requires knowledge of the ^{15}N chemical shift anisotropy (CSA) and of the ^{1}H-^{15}N internuclear distance. For the ^{15}N-CSA, a value of -160 ppm is commonly used for backbone relaxation analysis (Kay et al., 1989), although in some recent reports a slightly larger value of -170 ppm was chosen (Tjandra et al., 1996; Cordier et al., 1998). An even wider range of ^{15}N-CSA values (for a review see Fushman and Cowburn, 1998) was found in solid-state NMR studies of short peptides and model compounds. We therefore performed several calculations to verify whether individual adjustment of ^{15}N-CSA values for each residue can significantly improve the correspondence between experimental and calculated relaxation data (see lines 2, 9, and 16 of Table 3). Clearly, the per residue adjustment of the ^{15}N-CSA value generally entails a significant drop in the loss function; still model III provides the best fit. For models I and II, the optimized ^{15}N-CSA values moreover become unreasonably large (up to ca. $-190/-200$ ppm) while model III yields values of -176 ± 10 ppm, in good agreement with the experimentally derived values.

The results of the calculations with adjustable HN internuclear distances are shown in lines 3, 10, and 17 of Table 3. Again, the loss functions were significantly reduced for model II. An inspection of the obtained dynamic parameters, however, shows that the correlation times and order parameters become very similar to those provided by model III without adjustment of the internuclear distances. The order parameter S^2 and correlation time τ_e of model II in this case correspond to the order parameter S_s^2 and correlation time τ_s of model III. The adjustment of the internuclear distances merely compensates for the absence of the order parameter S_f^2 in model II. Thus, it is not surprising that the optimized distances obtained for model II are systematically higher by ca. 0.004 nm than the commonly accepted value of 0.102 nm.

In conclusion, the isotropic model III (line 15 in Table 3), accounting for nanosecond internal motions, provides a reasonable compromise between good fit and over-parametrization of the experimental data. Both cumulative and per residue loss functions are below their critical levels for the 95% quantile (except for the per residue loss function of Gly31). It follows that this model provides a good fit within the assumed uncertainties in the experimental data. Yet, further statistically meaningful reductions of the loss function (as verified by the F-test) are possible if further adjustable parameters are introduced into the model (see lines 16–19 in Table 3). This small mismatch between calculated and experimental relaxation data could be due to an actual over-simplification of the motional model or to residual small systematic errors in the experimental data which do not exceed the assumed errors (see Materials and methods). Sticking with the latter possibility, we confined our analysis to the simplest model (isotropic model III), which resulted in an overall rotation correlation time τ_R of 5.77 ± 0.15 ns. The rounded off τ_R value of 5.8 ns was then used for the further dynamic analysis of the individual backbone amide groups of (1–36)BR.

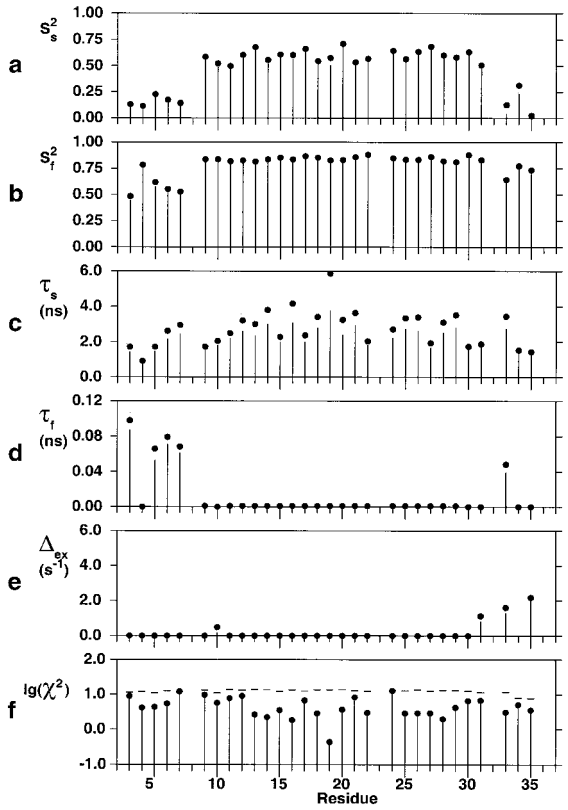

Figure 2. Results of the final model-free calculations for (1–36)BR. Molecular rotation was assumed to be isotropic with a correlation time of $\tau_R = 5.8$ ns and model function IV, which in the case of $\tau_f = 0$ reduces to model function III (see Table 2), was used throughout. A parameter for conformational exchange, Δ_{ex}, was required for residues 10, 31, 33 and 35. The correlation time τ_f for picosecond motions was resolved for residues 3, 5, 6, 7, 33 and 35. (a and b) Order parameters S_s^2 and S_f^2 for the nano- and picosecond motions, respectively. (c and d) Correlation times τ_s and τ_f for the nano- and picosecond motions. (e) Line broadening Δ_{ex} due to conformational exchange, valid for a ^{1}H Larmor frequency of 750 MHz. (f) Values of the per residue loss function χ^2. Horizontal bars indicate the critical values for the 95% quantile.

Model-free analysis

The results of the final model-free calculations are presented in Figure 2. Models I and II, with τ_R set to 5.8 ns, produce extremely high values of the loss function for all residues (data not shown) and are thus inappropriate throughout all of (1–36)BR. Residues 10–29 in the α-helical part of the protein exhibit good fits for model III. Figure 2 shows that the obtained values of the loss function are below their critical 95% levels for all these residues. The following average values and dispersions for the dynamic parameters were observed for the α-helical residues 9–29: $\langle S_s^2 \rangle = 0.60 \pm 0.05$, $\langle S_f^2 \rangle = 0.84 \pm 0.02$, $\langle \tau_s \rangle = 3.0 \pm 1.0$ ns. The inclusion of more model parameters was necessary for the residues in the N- and C-termini. Residues Gly31, Gly33, and Ser35 exhibit significant line broadening due to conformational exchange. T_2 values of Val34 measured at 600 and 750 MHz spectrometers turned out to be very low and inconsistent with the simple square dependence on the spectrometer field. This points to the strong line broadening due to conformational exchange for this NH and to the possible violation of the fast exchange limit assumption, which is essential for the square field dependence. Thus, no quantitative calculations of the line broadening were made for Val34 and T_2 values were not used for the model-free calculations for this residue. All residues in the C-terminus are thus clearly involved in motional processes on the micro- to millisecond time scale. Residues 3–7 in the N-terminus, on the contrary, exhibit good fits for the transverse relaxation rates at all magnetic fields without the need of an exchange parameter whereas the ^{15}N{^{1}H}-NOEs, as calculated by model III, are significantly higher than the experimental values. This is a clear indication for very fast motions on the time scale up to some 10 ps, as implied by model IV (Table 2). The use of model IV, with an extra fast correlation time τ_f, indeed reduces the per residue loss functions in the N-terminus by almost threefold. The inclusion of τ_f was also necessary for Gly33 in the C-terminus. Structural studies show that both termini are flexible and do not form part of the α-helix. It can therefore be assumed that their corresponding HN vector dynamics are described by a superposition of correlation time eigenvalues, which is different from the pseudo-global correlation time valid for the helical residues. However, the individual adjustment of the apparent τ_R for these residues does not lead to a considerable reduction in their loss functions. Only for Ser35 did the slow order parameter S_s^2 vanish, indicating that the relaxation data of this residue can indeed be described by the simplest model I with an individual apparent correlation time of ca. 1.6 ns.

Discussion

Conformational exchange in (1–36)BR

The results presented in Figure 2 indicate substantial conformational exchange on the micro- to millisecond time scale for the C-terminus of (1–36)BR, although our previous studies with variable CPMG echo delays (Orekhov et al., 1995) failed to detect these processes. It must be borne in mind, however, that the suppres-

sion of Δ_{ex} contributions to R_2 by the CPMG pulse train is limited to conformational exchange processes with relatively long exchange correlation times (on the millisecond time scale). Previous structural studies of the bacteriorhodopsin fragments (1–36) (Pervushin and Arseniev, 1992) and (1–71) (Pervushin et al., 1994) revealed no ordered structure for residues 33–36. Notably, the mobility of the hinge region (residues 33–39) of (1–71)BR is significantly lowered on changing the medium from SDS micelles to a (1:1) chloroform/methanol mixture. We propose that the chloroform/methanol mixture can stabilise tentative hydrogen bonds in different conformations of the C-terminus of (1–36)BR, providing an explanation for the observed relatively fast conformational exchange on the microsecond time scale.

Motions on the pico- and nanosecond time scales

The dynamics on the pico- and nanosecond time scales occurring in the N- and C- termini of (1–36)BR are complex. These residues show no ordered structure and the prerequisite of the model-free approach, i.e. uncorrelated internal and overall motions, might be invalid here. The model-free parameters should then be regarded merely as the parameters of a triple-exponential approximation of the actual complex autocorrelation function while the available experimental data does not suffice to separate global and internal motions for these terminal residues. Most probably, the anisotropy of the molecular tumbling and transient formation of hydrogen bonds for these residues result in a broad spectrum of correlation times on the nanosecond time scale. Local flexibility of those peptide groups, which are not involved in stable hydrogen bonds, could provide the explanation for the observed motions on the picosecond time scale.

The extensive nanosecond dynamics of the α-helical backbone amides of (1–36)BR as derived from the presented new set of relaxation measurements at several magnetic fields are in line with our previous dynamic studies of BR peptides performed at one magnetic field (Orekhov et al., 1995). In the work of Pervushin et al. (1995b), nanosecond motions were explained by the overdamped bending oscillations of the α-helix of (1–36)BR. Although motions of this kind most probably do occur in solution, the experimental order parameters S^2 (corresponding to amplitudes) and correlation times do not follow the trends expected from the bending model. The only definite result obtained from the analysis of the relaxation data for the α-helical residues of (1–36)BR is that a dynamic model must include at least two correlation times in the nanosecond time range to be consistent with the experimental data. We have also shown that these apparent additional nanosecond motions cannot be accounted for by the overall rotational anisotropy. The mean order parameter $\langle S_s^2 \rangle$ for the nanosecond motions of the α-helical residues with an average correlation time of some 3 ns is as low as 0.6, indicating that the amplitudes of these internal motions are quite substantial. Such high amplitudes, however, strongly suggest temporary ruptures of the α-helix. We therefore suggest that the α-helix in (1–36)BR exhibits fast transitions between folded and partially or completely unfolded states. Since the peptide remains in thermal equilibrium with the environment during the NMR experiments, these transitions represent the equilibrium helix-coil transitions. The low cooperativity of the helix-coil interconversion in (1–36)BR implies a high content of partially unfolded states of the peptide. For such states, the model-free approach assumption of uncorrelated overall and internal motions could fail. Moreover, the anisotropy of the overall molecular rotation in the partially unfolded states, which, in contrast to the folded state, cannot be quantified due to the large variety of unknown conformations, probably creates a broad distribution of effective overall correlation times. It is therefore not clear whether the observed correlation times τ_s of the nanosecond internal motions represent the true correlation times of the helix-coil transitions or whether they are only the manifestation of the motional anisotropy in the different unfolded states. In the latter case, the helix-coil transitions could occur on a slower time scale.

Conclusions

We have shown that heteronuclear NMR relaxation measurements can provide valuable information about the early events of protein folding and help us to detect and quantify equilibrium helix-coil transitions in (1–36)BR. The obtained results are in good agreement with current theoretical and experimental data on the kinetics of helix-coil transitions (see Korzhnev et al., 1999b and references therein). The possibility to simultaneously observe the relatively stable α-helix (by applying regular NMR structure determination procedures) and the transitions between this α-helix and a set of partially unfolded conformations (by applying the model-free approach to NMR relaxation data) is a result of the low cooperativity of the helix-coil tran-

sitions in low polar solvents. In our previous study of (1–36)BR and (1–71)BR (Orekhov et al., 1995) the nanosecond dynamics of these peptides were observed both in a chloroform/methanol mixture and in SDS micelles. This indicates that similar helix-coil transitions can also be expected for native bacteriorhodopsin in membranes, although the interaction between helices could affect the thermodynamics and kinetics of these transitions.

Acknowledgements

This work was supported by Russian Foundation for Basic Research grants 96-04-00054, 96-04-50893, by ISSEP grants a97-969, a98-2221 and by the Deutsche Forschungsgemeinschaft grant Ke-147/31.

References

Abragam, A. (1961) *The Principles of Nuclear Magnetism*, Oxford University Press, London.
Baldwin, R.L. (1989) *Trends Biochem. Sci*., **14**, 291–294.
Beloborodov, I.S., Orekhov, V.Yu. and Arseniev, A.S. (1998) *J. Magn. Reson*., **132**, 328–329.
Bracken, C., Carr, P.A., Cavanagh, J. and Palmer, A.G. (1999) *J. Mol. Biol*., **285**, 2133–2146.
Chou, P.Y. and Scheraga, H.A. (1971) *Biopolymers*, **10**, 657–680.
Clore, G.M., Szabo, A., Bax, A., Kay, L.E., Driscoll, P.C. and Gronenborn, A.M. (1990) *J. Am. Chem. Soc.*, **112**, 4989–4991.
Cordier, F., Caffrey, M., Brutscher, B., Cusanovich, M.A., Marion, D. and Blackledge, M. (1998) *J. Mol. Biol*., **281**, 341–361.
Daggett, V. and Levitt, M. (1992) *J. Mol. Biol.*, **223**, 1121–1138.
Farrow, N.A., Muhandiram, R., Singer, A.U., Pascal, S.M., Kay, C.M., Gish, G., Shoelson, S.E., Pawson, T., Forman-Kay, J.D. and Kay, L.E. (1994) *Biochemistry*, **33**, 5984–6003.
Fushman, D. and Cowburn, D. (1998) *J. Am. Chem. Soc*., **120**, 7109–7110.
Garcia de la Torre, J. and Bloomfield, V.A. (1981) *Quart. Rev. Biophys*., **14**, 81–139.
Gruenewald, B., Nicola, C.U., Lustig, A., Schwarz, G. and Klump, H. (1979) *Biophys. Chem.*, **9**, 137–147.
Hirota, N., Mizuno, K. and Goto, Y. (1997) *Protein Sci*., **6**, 416–421.
Kahn, T.W. and Engelman, D.M. (1992) *Biochemistry*, **31**, 6144–6151.
Karplus, M. and Weaver, D.L. (1994) *Protein Sci*., **3**, 650–668.
Kay, L.E., Torchia, D.A. and Bax, A. (1989) *Biochemistry*, **28**, 8972–8979.
Korzhnev, D.M., Orekhov, V.Yu. and Arseniev, A.S. (1997) *J. Magn. Reson.*, **127**, 184–191.
Korzhnev, D.M., Orekhov, V.Yu., Arseniev, A.S., Gratias, R. and Kessler, H. (1999) *J. Phys. Chem. B*, **103**, 7036-7043.
Korzhnev, D.M., Orekhov, V.Yu. and Arseniev, A.S. (1999b) *J. Biomol. NMR*, **14**, 357–368.
Lipari, G. and Szabo, A. (1982) *J. Am. Chem. Soc.*, **104**, 4546–4559.
Luo, P. and Baldwin, R.L. (1997) *Biochemistry*, **36**, 8413–8421.
Mandel, A.M., Akke, M. and Palmer, A.G. (1995) *J. Mol. Biol*., **246**, 144–163.
Marti, T. (1998) *J. Biol. Chem.*, **273**, 9312–9322.
Miick, S.M., Casteel, K.M. and Millhauser, G.L. (1993) *Biochemistry*, **32**, 8014–8021.
Orekhov, V.Yu., Pervushin, K.V., Korzhnev, D.M. and Arseniev, A.S. (1995) *J. Biomol. NMR*, **6**, 113–122.
Orekhov, V.Yu., Nolde, D.E., Golovanov, A.P., Korzhnev, D.M. and Arseniev, A.S. (1996) *Appl. Magn. Reson.*, **9**, 581–588.
Palmer, A.G., Williams, J. and McDermott, A. (1996) *J. Phys. Chem.*, **100**, 13293–13310.
Pervushin, K.V. and Arseniev, A.S. (1992) *FEBS Lett*., **308**, 190–196.
Pervushin, K.V., Orekhov, V.Yu., Popov, A.I., Musina, L.Yu. and Arseniev, A.S. (1994) *Eur. J. Biochem*., **219**, 571–583.
Pervushin, K.V. and Arseniev, A.S. (1995a) *Bioorg. Khim.*, **21**, 83–111.
Pervushin, K.V., Orekhov, V.Yu., Korzhnev, D.M. and Arseniev, A.S. (1995b) *J. Biomol. NMR*, **5**, 383–396.
Phillips, C.M., Mizutani, Y. and Hochstrasser, R.M. (1995) *Proc. Natl. Acad. Sci. USA*, **92**, 7292–7296.
Popot, J.L., Gerchman, S.E. and Engelman, D.M. (1987) *J. Mol. Biol.*, **198**, 655–676.
Reeves, L.W. (1975) In *Dynamic Nuclear Magnetic Resonance Spectroscopy* (Eds. Jackman, L.M. and Cotton, F.A.), Academic Press, New York, NY, pp. 83–130.
Scholtz, J.M. and Baldwin, R.L. (1992) *Annu. Rev. Biophys. Biomol. Struct.*, **21**, 95–118.
Schurr, J.M., Babcock, H.P. and Fujimoto, B.S. (1994) *J. Magn. Reson.*, **A105**, 211–224.
Thompson, P.A., Eaton, W.A. and Hofrichter, J. (1997) *Biochemistry*, **36**, 9200–9210.
Tjandra, N., Wingfield, P., Stahl, S. and Bax, A. (1996) *J. Biomol. NMR*, **8**, 273–284.
VanGeet, A.L. (1970) *Anal. Chem.*, **42**, 679–680.
Williams, S., Causgrove, T.P., Gilmanshin, R., Fang, K.S., Callender, R.H., Woodruff, W.H. and Dyer, R.B. (1996) *Biochemistry*, **35**, 691–697.
Woessner, D.E. (1962) *J. Chem. Phys.*, **37**, 647–654.